Histone Acetyltransferase GCN5 Regulates Osteogenic Differentiation of Mesenchymal Stem Cells by Inhibiting NF-κB

Article *in* Journal of bone and mineral research: the official journal of the American Society for Bone and Mineral Research · September 2015

DOI: 10.1002/jbmr.2704

6 authors, including:

Yongsheng Zhou
Peking University School of Stomatology
54 PUBLICATIONS **507** CITATIONS

SEE PROFILE

ORIGINAL ARTICLE

JBMR®

Histone Acetyltransferase GCN5 Regulates Osteogenic Differentiation of Mesenchymal Stem Cells by Inhibiting NF-κB

Ping Zhang,[1] Yunsong Liu,[1] Chanyuan Jin,[1] Min Zhang,[1] Fuchou Tang,[2] and Yongsheng Zhou[1,3]

[1]Department of Prosthodontics, Peking University School and Hospital of Stomatology, Beijing, China
[2]Biodynamic Optical Imaging Center, College of Life Sciences, Peking University, Beijing, China
[3]National Engineering Laboratory for Digital and Material Technology of Stomatology, Peking University School and Hospital of Stomatology, Beijing, China

ABSTRACT

As the most well-studied histone acetyltransferase (HAT) in yeast and mammals, general control nonderepressible 5 (GCN5) was documented to play essential roles in various developmental processes. However, little is known about its role in osteogenic differentiation of mesenchymal stem cells (MSCs). Here, we detected the critical function of GCN5 in osteogenic commitment of MSCs. In this role, the HAT activity of GCN5 was not required. Mechanistically, GCN5 repressed nuclear factor kappa B (NF-κB)-dependent transcription and inhibited the NF-κB signaling pathway. The impaired osteogenic differentiation by GCN5 knockdown was blocked by inhibition of NF-κB. Most importantly, the expression of GCN5 was decreased significantly in the bone tissue sections of ovariectomized mice or aged mice. Collectively, these results may point to the GCN5-NF-κB pathway as a novel potential molecular target for stem cell mediated regenerative medicine and the treatment of metabolic bone diseases such as osteoporosis. © 2015 American Society for Bone and Mineral Research.

KEY WORDS: GCN5; MSCS; NF-κB; OSTEOGENIC DIFFERENTIATION; OSTEOPOROSIS

Introduction

Human mesenchymal stem cells (MSCs) can be differentiated into osteoblasts, chondrocytes and adipocytes in vitro depending on culture conditions.[1–3] Due to their ease of isolation and lack of immunogenicity, MSCs have shown strong potential in bone regeneration and tissue engineering. The capacity of MSCs to repair skeletal defects was originally evaluated in experimental animal models and subsequently in human osteogenesis imperfecta patients.[4] Recent growing evidence has revealed that the final cell fate decision of MSCs relies on an orchestrated activation of lineage-specific genes and repression. For example, Runx2 and Osx are considered master transcription factors for osteogenic differentiation,[5–8] whereas the nuclear hormone receptor peroxisome proliferator-activated receptor γ (PPARγ) is a critical adipogenic regulator promoting MSC adipogenesis.[9,10] Multiple signaling pathways, including the Hedgehog, Notch, WNT, BMP, and FGF pathways, have also been demonstrated to participate in the differentiation of an osteoblast progenitor to a committed osteoblast.[11–18] In order to effectively harness MSCs for clinical use, it is crucial to gain a better understanding of the molecular mechanism underlying the differentiation of MSCs.

The transcription factor nuclear factor kappa B (NF-κB) is a critical regulator of inflammation and immune signals.[19,20] Recently, NF-κB was reported to play important roles in skeletal remodeling and bone homeostasis by controlling the differentiation of osteoprogenitor cells.[21–24] Selective inhibition of NF-κB was demonstrated to block RANKL-induced osteoclastogenesis both in vitro and in vivo and prevent inflammatory bone destruction in vivo.[25] Moreover, RelA/p65, a subunit of NF-κB, was demonstrated to promote osteoclast differentiation by blocking RANKL-induced apoptosis.[26] In addition, activation of NF-κB has been shown to prevent osteogenic differentiation of MSCs and postnatal bone formation in vivo.[22,24] Thus, targeting NF-κB may both promote bone formation and inhibit bone resorption, and factors influencing its expression or transcriptional activity may be potential targets for the regulation of osteogenic differentiation.

General control nonderepressible 5 (GCN5) was identified as the first histone acetyltransferase (HAT) related to transcriptional regulation in 1996,[27] and its biological functions have since been well-studied. This HAT performs both global and

Received in original form May 13, 2015; revised form August 26, 2015; accepted September 3, 2015. Accepted manuscript online September 07, 2015.
Address correspondence to: Yongsheng Zhou, D.D.S., Ph.D., Department of Prosthodontics, Peking University School and Hospital of Stomatology, 22 Zhongguancun South Avenue, Haidian District, Beijing 100081, China. E-mail: kqzhouysh@hsc.pku.edu.cn
*PZ and YL contributed equally to this work.
Additional Supporting Information may be found in the online version of this article.

Journal of Bone and Mineral Research, Vol. xx, No. xx, Month 2015, pp 1–12
DOI: 10.1002/jbmr.2704

locus-specific histone acetylation, as well as acetylation of nonhistone proteins such as transcriptional factors[27–29] HATs are known to serve as coactivators of transcription and play important roles for gene activation.[30] Although enrichment of GCN5 has also been associated with genes that are repressed during stress[31–33] no mechanism for how GCN5 contributes to gene repression has been characterized. Although a few prior studies have elucidated the role of GCN5 in regulating bone morphogenetic protein signaling and mouse skeleton development,[34,35] little is known regarding how GCN5 affects bone formation and whether this HAT is involved in the most common bone disease osteoporosis.

In the present study, we first identified that GCN5 was essential for the osteogenic differentiation of MSCs and played an important role in osteoporosis. Mechanistically, GCN5 inhibited NF-κB signaling, which was demonstrated as a negative regulator of osteoblast function. Notably, the GCN5-promoted osteogenic differentiation was found to be separable from its HAT activity, establishing this function as a distinct property of GCN5.

Materials and Methods

Isolation and culture of MSCs

Primary human adipose-derived stem cells and bone marrow MSCs were purchased from ScienCell Research Laboratories (Carlsbad, CA, USA). To induce differentiation, MSCs were cultured in osteogenic media containing 100 mM/mL ascorbic acid, 2 mM β-glycerophosphate, and 10 nM dexamethasone.

Bone marrow samples were collected from sham, ovariectomized (OVXed), younger (2-month-old) and older (16-month-old) mice by flushing the femurs and tibias with complete medium containing Dulbecco's Modified Eagle's Medium (DMEM) (Invitrogen, Carlsbad, CA, USA), 10% fetal calf serum (FBS) (PAA Laboratories GmbH, Linz, Austria), and penicillin/streptomycin (Invitrogen). The bone marrow suspension was concentrated, washed twice in DMEM, and then cultured at 37°C with 5% CO_2 atmosphere. Cells were collected after 2 weeks when the MSCs had expanded.

Viral infection

For viral packaging, HEK293T cells at 80% confluency were cotransfected with the lentiviral transfer plasmid (pLNB) vectors with a mutant chicken β-actin (CBA) promoter for gene expression or shRNAs, the lentiviral packaging plasmid (psPAX2) (Addgene, Cambridge, MA, USA) and the VSV-G-expressing envelope plasmid (pVSV-G) (Clontech Laboratories, Palo Alto, CA, USA) using the PolyJet Transfection Reagent (SignaGen Laboratories, Rockville, MD, USA) according to the manufacturer's instructions. The cell culture supernatant was collected at 36, 48, and 60 hours after transfection, centrifuged, and filtered through an Acrodisc filter with a 0.45-μm polyvinylidene fluoride (PVDF) membrane (Pall Corporation, Port Washington, NY, USA) to remove cellular debris. The viral particles were then precipitated by centrifugation with PEG-it (System Biosciences [SBI], Mountain View, CA, USA). The concentrated lentiviral particles were titered, aliquotted, and stored at –70°C until ready for use.

In order to facilitate tracking of the knockdown efficiency, we generated lentiviral plasmids for coexpression of green fluorescent protein (GFP) or red fluorescent protein (RFP) with the target shRNA separately. We constructed a GCN5 RNA interference plasmid with a lentivirus vector expressing RFP, and the recombinant p65 RNA interference vector was established with a lentivirus vector expressing GFP.

The shRNA target sequences were: scrambled non-target shRNA, GTCTCCACGCGCAGTACATTT; GCN5sh#1, CCATTCATTCC CTGGCATTAA; GCN5sh#2, GGCTACCTACAAGGTCAATTA; RelA sh#1, GCCTTAATAGTAGGGTAAGTT; and RelAsh#2, GCGCATC CAGACCAACAACAA.

ALP staining

After 7 days of culture, cells were washed with PBS three times and then fixed in 4% paraformaldehyde at room temperature (RT) for 10 min. Subsequently, the cells were washed in PBS three times, incubated with a 5-bromo-4-chloro-3-indolyl phosphate–4-nitro blue tetrazolium (BCIP/NBT) staining kit (CWBIO, Beijing, China) solution for 15 min at RT and rinsed with water.

Quantification of ALP activity

Cells from six-well culture plates were washed three times with ice-cold PBS and then treated with 500 μL/well of 1% Triton X-100 (Sigma, St. Louis, MO, USA) for 5 min at RT for cell lysis. Cells were collected with a cell scraper, sonicated on ice, and then centrifuged at 4°C for 30 min at 13000 g. The supernatants were used for determining protein concentration using a bicinchoninic acid (BCA) protein assay reagent (Prod#23225; Pierce Thermo Scientific, Waltham, MA, USA) and measuring ALP activity. ALP activity in cell lysates was measured using an ALP assay kit (A059-2; Nanjing Jiancheng Bioengineering Institute, Nanjing, China) and normalized by the protein content. Each experimental condition was repeated three times.

Alizarin Red staining and quantification

Analysis of mineralization was determined by Alizarin Red staining. Cells were first rinsed with Milli-Q water (Millipore, Billerica, MA, USA), fixed for 30 min in 70% ethanol at 4°C, and then rinsed with Milli-Q water. Calcium deposition was then visualized after incubation with 2% Alizarin Red S pH 4.2. Alizarin Red S was extracted by destaining with hexadecyl pyridinium chloride monohydrate, and mineral accumulation was quantified on a microplate reader at 562 nm.

Real-time quantitative PCR

Total RNA was extracted with TRIZOL reagent (Invitrogen) and precipitated with ethanol. To exclude potential contamination of DNA, RNA was treated with DNase I for 30 min at 37°C. cDNA was synthesized from 0.5 to 2 μg of RNA with oligonucleotide (dT) 18 primers by using the Quantscript RT Kit (Tiangen, Beijing, China).

Real-time quantitative PCR (RT-qPCR) was performed on an Eppendorf Mastercycler ep realplex (Eppendorf, Hamburg, Germany) using the Fast-Start Universal SYBR Green Master Mix (Roche Applied Science, Mannheim, Germany). Reactions were carried out in a total volume of 20 μL containing 2 μL of 1:10 diluted template cDNA, 10 μL of 2 × SYBR green PCR Master Mix (Roche Applied Science, Mannheim, Germany) and 100 nM of each primer. The following amplification program was used in all PCRs: 95°C for 10 min, followed by 40 cycles of 15 s at 95°C, and 1 min at 60°C. The specificity of each amplified reaction was verified by a dissociation curve (melting curve) analyses after 40 cycles, which was carried out by heating the amplicon from 60°C

to 95°C. Moreover, the specificity of the PCR product was further confirmed by 2% agarose gel electrophoresis. Each sample was analyzed in triplicate wells, and no-template controls (without cDNA in the PCR) were included. Data were collected and quantitatively analyzed using realplex software.

The primer sequences used for the amplification of human *GAPDH*, *ICAM1*, *IL6*, *IL8*, *RUNX2*, *SP7*, *BGLAP*, *ALP*, and *COL1A1*, as well as mouse *Gapdh, Gcn5*, *Il6*, *Il8*, and *Icam1* for RT-qPCR were as follows: human *GAPDH*, (F) AAGGAGTAAGACCCCTGGACCA, (R) GCAACTGTGAGCAGGGGAGATT; *RUNX2*, (F) ACTACCAGCCACCGAGACCA, (R) ACTGCTTGCAGCCTTAAATGACTCT; *SP7*, (F) AACAGGAGTGGAGCTGGCCT, (R) GCCATAGTGAACTTCCTCCT GGG; *BGLAP*, (F) CACCATGAGAGCCCTCACACTC, (R) CCTGCTTGG ACACAAAGGCTGC; *ALP*, (F) TGTGTGGGGTGAAGGCCAAT, (R) TCGTGGTGGTCACAATGCCC; *COL1A1*, (F) TGGTCCCAAGGGTAACAGCG, (R) AACACCAACAGGGCCAGGCT; *Il6*, (F) GCCAGAGCT GTGCAGATGAGT, (R) AGCAGGCTGGCATTTGTGGT; *IL8*, (F) ACCACACTGCGCCAACACAG, (R) TGCACCCAGTTTTCCTTGGGG; *ICAM1*, (F) AGTGTGACCGCAGAGGACGA, (R) GGCGCCGG AAAG CTGTAGAT; *TNF*, (F) GCCCAGGCAGTCAGATCATCTTC, (R) ACAGGCTTGTCACTCGGGGT; mouse *Gapdh*, (F) ACAGCAACTCCCACTCTTCCAC, (R) AGTTGGGATAGGGCCTCTCTTG; *Gcn5*, (F) TGGAAAAACCCCAAGCCCCC, (R) GGGACACATGGTCCGCCAAA; *Il6*, (F)TTCCTCTCTGCAAGAGACTTCC, (R) TTGTGAAGTAGGGAA GGCCG; *Il8*, (F) CTGCTGGCTGTCCTTAACCT, (R) GTCACAGGGACGGACGAAGA; and *Icam1*, (F)CCACTGCCTTGGTAGAGGTG, (R) GTCAGGACCGGAGCTGAAAA.

Chromatin immunoprecipitation assay

Briefly, 2×10^7 cells were cross-linked with 1% formaldehyde, resuspended in lysis buffer on ice for 3 min and fragmented by sonication. Soluble chromatin was then diluted and subjected to immunoprecipitation with the indicated antibodies. Immune complexes were then precipitated with Protein A/G Dynabeads (Life Technologies, Carlsbad, CA, USA), washed sequentially with RIPA (0.5 mM EGTA, 140 mM NaCl, 10 mM Tris-HCl, pH 7.5, 1% TritonX-100, 0.01% SDS, 1 mM EDTA and protease inhibitor) and TE (50 mM NaCl, 5 mM EDTA, and 50 mM Tris-HCl [pH 8.0]) buffer. After the cross-linking was reversed, the DNA was purified and subjected to RT-qPCR analysis. Sequences of chromatin immunoprecipitation (ChIP) primers were as follows: *IL6*, (F) AAGGTTTCCAATCAGCCCCA, (R) TTCTCTTTCGTTCCCGGTGG; *IL8*, (F) CTTGAGGCATCTGTGAGGGA, (R) ATGAGCCCCTTGACCAT GTG; and *ICAM1*, (F) ATTCAAGCTTAGCCTGGCCG, (R) ATTT CCGGACTGACAGGGTG.

Coimmunoprecipitation and Western blot

Nuclear extraction, total protein extraction, and Western blot were performed as described.[36] The antibodies used were anti-GCN5, anti-RelA, anti-H3, and anti-H3K9 (Cell Signaling, Danvers, MA, USA); anti-NF-kB p65 (acetyl K310) and anti-NF-kB p65 (Abcam, Cambridge, UK); anti-actin and anti-tubulin (Santa Cruz Biotechnology, Dallas, TX, USA). For immunoprecipitation, cells were harvested and then lysed in a Nonidet P-40 buffer supplemented with a Complete protease inhibitor mixture (Roche). Whole-cell lysates were used for immunoprecipitation with the indicated antibodies.

Bone formation in vivo

Nude mouse implantation was performed as described.[37] Specimens of each group were harvested at 6 weeks after implantation, and animals in each group were euthanized by CO_2 asphyxiation. The bone constructs were fixed in 4% paraformaldehyde and then decalcified for 10 days in 10% EDTA (pH 7.4). After decalcification, the specimens were dehydrated and subsequently embedded in paraffin. Sections (5-mm thickness) were stained with hematoxylin and eosin (H&E) and Masson's trichrome stain.

Sample preparation and histomorphometric analyses were performed as described.[38] For quantification of bone-like tissue, 10 images of each sample were taken randomly (Olympus, Tokyo, Japan) and SPOT 4.0 software (Diagnostic Instruments, Sterling Heights, MI, USA) was used to measure the area of new bone formation versus total area.

Micro–CT analyses of mice

C57BL/6 mice were obtained from The Jackson Laboratory (Bar Harbor, ME, USA). Mice were maintained in a pathogen-free facility on a 12-hour light/dark cycle with water and food provided *ad libitum*. All work was approved by the Peking University Biomedical Ethics Committee Experimental Animal Ethics Branch. Five-month-old mice were sham-operated (sham) or ovariectomized (OVXed), and the OVXed mice presented osteoporosis as described.[39] Mice were allowed 3 months to recover from the ovariectomy surgery and then euthanized for the related assays. Because osteoporosis is also an age-related marker in mice,[40] female 2-month-old mice (young) and 16-month-old mice (old) were used in the study.

The proximal femur and tibia thoroughly dissected free of soft tissue was fixed with 4% paraformaldehyde for 24 hours and subsequently washed with 10% sucrose solution. Twelve hours later, images were scanned at a resolution of 8.82 μm, with tube voltage of 80 kV, tube current of 500 μA, and exposure time of 1500 ms. A typical examination consisted of a scout view, selection of the examination volume, automatic positioning, measurement, offline reconstruction, and evaluation. Two-dimensional images were used to generate 3D reconstructions using multimodal 3D visualization software (Inveon Research Workplace, Siemens, Munich, Germany) supplied by the micro–computed tomography (μCT) system.

To evaluate the mass and microarchitecture in bone between different groups, μCT was undertaken using an Inveon MM system (Siemens). Images were acquired at an effective pixel size of 8.82 μm, voltage of 80 kV, current of 500 μA, and exposure time of 1500 ms in each of the 360 rotational steps. Parameters were calculated using an Inveon Research Workplace (Siemens) as follows: bone volume/total volume (BV/TV), trabecular thickness (Tb.Th), trabecular number (Tb.N), and trabecular separation (Tb.Sp) in the trabecular region (1 to 2 mm distal to the proximal epiphysis) according to guidelines set by the American Society for Bone and Mineral Research (ASBMR).[41]

Histology and immunofluorescence staining of MSCs and bone sections

MSCs were incubated with monoclonal anti-nestin (Lifespan Bio Sciences, 1:500) at 4°C overnight. After washing with PBS three times, the cells were incubated with appropriate secondary antibodies (1:100 dilution; Jackson ImmunoResearch, West Grove, PA, USA) in the dark at room temperature for 1 hour. The cells were imaged with a confocal laser scanning microscope (LSM510; Carl Zeiss, Oberkochen, Germany).

Bones were fixed in 4% paraformaldehyde at 4°C under constant agitation for 3 days and then decalcified in 14% EDTA solution (EDTA dissolved in Milli-Q water, with pH adjusted to 7.1 with ammonium hydroxide) at 4°C or room temperature under constant agitation for 3 to 5 days (fresh 14% EDTA solution was exchanged every 24 hours). Bones were then washed in PBS for 2 hours, soaked in 30% sucrose in PBS at 4°C under constant agitation overnight, and finally embedded in 22-oxa-1,25-dihydroxyvitamin D_3 optimum cutting temperature (OCT) compound. Free-floating sections (30-μm thick) were processed for immunohistochemistry as described[42] with minor modifications. The anti-GCN5 antibody (1:100 dilution; Abcam) and the anti-p65 antibody (1:100 dilution; Abcam) were applied overnight at 4°C. The secondary antibody used was Alexa Fluor 546–labeled-goat anti-rabbit IgG (1:2000 dilution; Invitrogen). Cell nuclei were counterstained with Hoechst 33258 (Invitrogen). Fluorescence images were acquired with a confocal laser scanning microscope (LSM510).

Statistical analysis

All statistical analyses were performed using the GraphPad scientific software for Windows (GraphPad Software, Inc., La Jolla, CA, USA). Comparisons between two groups were analyzed by independent two-tailed Student's *t* tests, and comparisons between more than two groups were analyzed by one-way ANOVA followed by a Tukey's post hoc test. Data were expressed as the mean ± standard deviation (SD) of 3 to 10 experiments per group. Values of $p < 0.05$ were considered statistically significant.

Results

Knockdown of GCN5 inhibits differentiation of MSCs into osteoblast cells

To evaluate the potential role of GCN5 in the process of osteogenic differentiation, we first generated a stable cell line with lentiviruses expressing GCN5 shRNA. The knockdown efficiency was confirmed by immunofluorescence and Western blotting (Supplemental Fig. 1A, Fig. 1*A*). After culturing the MSCs in osteogenic media for 7 days, ALP activity was detected and found to be significantly suppressed by GCN5 knockdown (Fig. 1*B*, *C*). Moreover, the extracellular matrix mineralization, as determined by Alizarin Red S staining and quantification, was also impaired in GCN5 knockdown cells at 2 weeks after osteogenic induction (Fig. 1*D*, *E*). To confirm that GCN5 depletion inhibited osteogenic differentiation, we investigated several osteogenic markers when MSCs were treated with osteogenic stimulation. As shown in Fig. 1*F–I*, in contrast to the control cells, knockdown of GCN5 resulted in significantly decreased mRNA expression levels of *RUNX2*, *SP7*, *BGLAP*, and *COL1A1*. In addition, the osteogenic differentiation of MSCs could also be blocked with another independent GCN5 shRNA fragment but not with a random shRNA, excluding the possibility of off-target effects (Supplemental Fig. 1B–G). Taken together, these results indicated that GCN5 knockdown inhibited osteogenic differentiation in vitro.

HAT activity of GCN5 is dispensable for its role in osteogenic differentiation

In order to further verify the function of GCN5 in the osteogenic differentiation process, we next established the GCN5 rescue cell line with the vector, flag-GCN5 (wild-type [WT]) and flag-GCN5Y621A/P622A (a GCN5 catalytically inactive acetyltransferase mutant)[43] (Supplemental Fig. 2A, Fig. 2*A*). As shown in Fig. 2*B*, *C*, not only WT GCN5 but also the catalytic mutant of GCN5 could promote the ALP activity in response to osteogenic stimulation. Similarly, when MSCs were treated with osteogenic media at 2 weeks, both WT and mutant GCN5 could enhance the formation of mineralization nodules (Fig. 2*D*, *E*). Thus, the regulation of osteogenic differentiation by GCN5 appeared to be independent of its HAT activity. In addition, we detected the expression of osteogenesis-associated genes in the GCN5 rescue cell line under osteogenic induction. These genes were upregulated in both WT and the mutant GCN5-overexpressing cells compared to the control cells (Fig. 2*F–H*, Supplemental Fig. 2*B*, *C*). Together, these results demonstrated that GCN5 promotes osteogenic differentiation independently of its HAT activity.

GCN5 is responsible for degradation of RelA and suppression of the NF-κB signaling pathway

To investigate the molecular mechanism by which GCN5 promotes osteogenic differentiation of MSCs, we screened several signaling pathways and key regulators of MSC differentiation. Unexpectedly, we found that GCN5 was responsible for the inhibition of NF-κB signaling. GCN5-deficient cells showed increased expression of NF-κB–targeted genes, such as *ICAM1* and *TNF*, as well as *IL6* and *IL8* (Fig. 3*A*, *B*; Supplemental Fig. 3*A*, *B*). Detection of the expression of NF-κB targets in GCN5 rescue cells revealed that both WT and mutant GCN5 effectively inhibited NF-κB–regulated genes (Fig. 3*C*, *D*; Supplemental Fig. 3C, D). Moreover, GCN5 suppressed NF-κB–dependent transcription, as determined by the NF-κB–dependent luciferase reporter assay (Fig. 3*E*). We also examined p65 recruitment to the promoters of the indicated targeted genes using the ChIP assay. The deficiency of GCN5 was found to lead to increased promoter occupancy by p65 (Fig. 3*F*, *G*; Supplemental Fig. 3E). To further investigate the role of GCN5 in the inhibition of the NF-κB pathway, Western blot assays were first conducted to detect the protein level of p65 in GCN5-deficient cells. Knockdown of GCN5 increased the nuclear protein level of p65 (Fig. 3*H*). By contrast, p65 levels were decreased in both WT and catalytically inactive mutant GCN5 rescue cells, whereas MG132 treatment could reverse the GCN5-induced decrease of p65 (Fig. 3*I*). As acetylation reportedly has been associated with increased NF-κB target gene transcription and is required for p65 activation,[44,45] we next investigated the p65 (acetyl K310) levels in both GCN5 knockdown and WT GCN5 overexpression cells. As shown in Supplemental Fig. 3F, G, the p65 acetylation levels was positively correlated with the p65 levels in GCN5-deficient and GCN5-overexpressing cells. Moreover, analyses using a coimmunoprecipitation (Co-IP) assay was conducted to verify the interaction between p65 and GCN5 (Supplemental Fig. 3H). As a whole, these results suggested that GCN5 inhibited NF-κB signaling by mediating the proteasomal degradation of p65.

Regulation of osteogenic differentiation by GCN5 is NF-κB–dependent

In order to clarify the functional connection between GCN5 and NF-κB signaling in osteogenic differentiation, we generated lentiviruses expressing p65 shRNA in GCN5 knockdown cells. As shown in Fig. 4*A* and Supplemental Fig. 4A, p65 was effectively

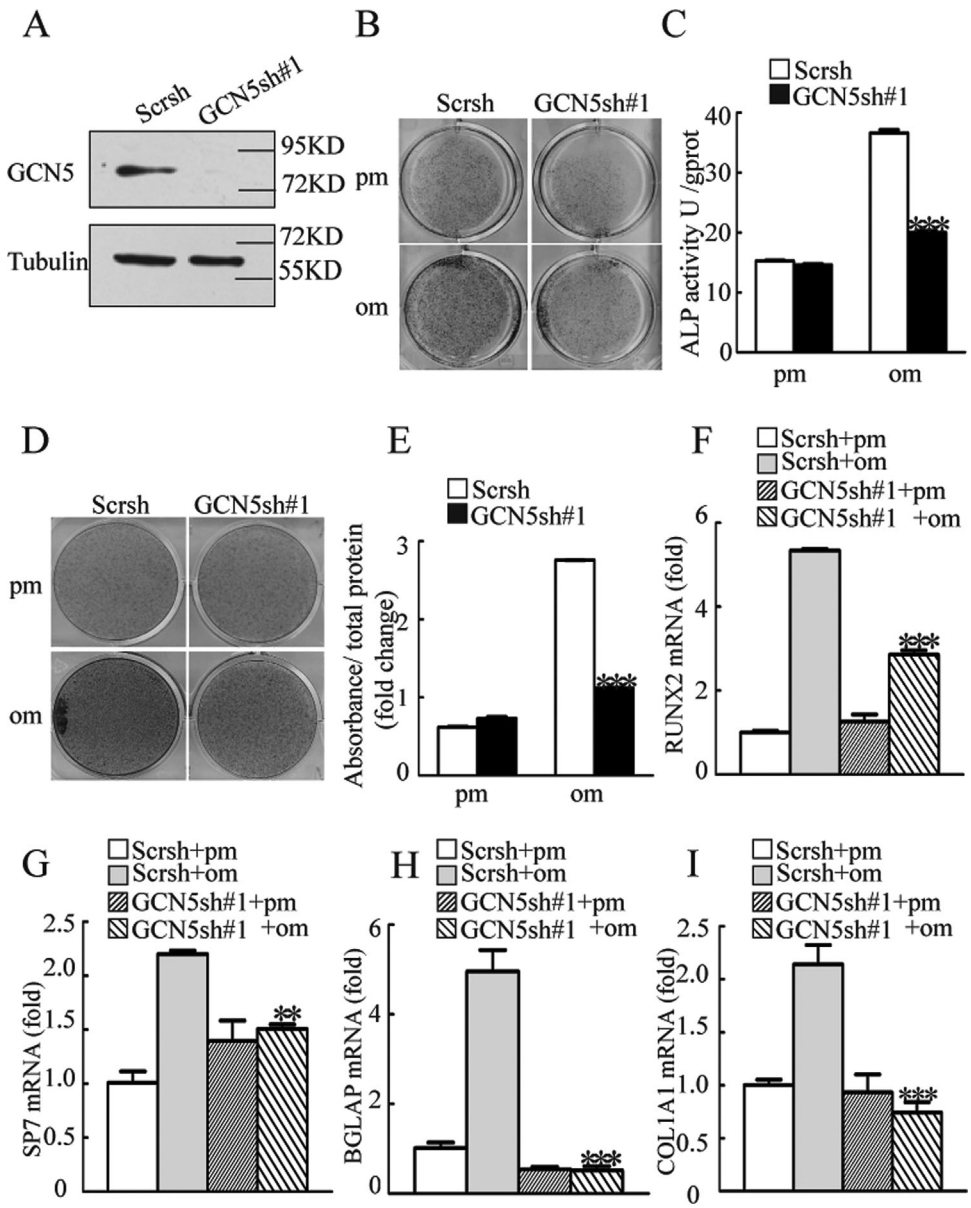

Fig. 1. Knockdown of GCN5 inhibits the osteogenic differentiation of MSCs. (*A*) Knockdown of GCN5 was validated by Western blot. (*B–C*) GCN5 knockdown decreased ALP activity in MSCs. Control or GCN5 knockdown cells were treated with proliferation or osteogenic media for 7 days for ALP staining (*B*), and cellular extracts were prepared to quantify ALP activity (*C*). (*D*, *E*) Knockdown of GCN5 inhibited mineralization in MSCs. Cells with or without GCN5 knockdown were treated with proliferation or osteogenic media for 14 days, and then calcium deposition was observed using Alizarin Red S staining (*D*) and quantified (*E*). The knockdown of GCN5-inhibited expression levels of *RUNX2* (*F*), *SP7* (*G*), *BGLAP* (*H*), and *COL1A1* (*I*) in MSCs were determined by RT-qPCR. All data are shown as the mean ± SD, $n = 3$. $^{**}p < 0.01$, $^{***}p < 0.001$. pm = proliferation media; om = osteogenic media; Scrsh = control cells; GCN5sh = GCN5 knockdown cells.

knocked down as determined by fluorescence and Western blot analyses. When cells were treated with osteogenic media, the decrease of osteogenic differentiation ability by GCN5 knockdown was effectively reversed in GCN5 and p65 double knockdown cells, which was indicated by ALP quantification (Fig. 4*B*). In addition, the decreased expression of *RUNX2* caused by GCN5 deficiency was also blocked by inhibition of p65 (Fig. 4*C*). Upon treatment of MSCs with the NF-κB inhibitor BAY 11–7082, NF-κB transcriptional activity showed a significant decrease (Supplemental Fig. 4B). Next, we treated GCN5 knockdown cells in the absence or presence of BAY 11–7082 in osteogenic media. As shown in Fig. 4*D*, inhibition of NF-κB activity could reverse the decrease in osteogenic differentiation caused by GCN5 knockdown. These results suggested that NF-κB was involved in the GCN5-regulated osteogenic differentiation process.

To further support this speculation, we examined whether the knockdown of GCN5 and p65 affected MSC-mediated bone formation in vivo. GCN5 knockdown, GCN5/p65 knockdown or negative control cells were mixed with collagen carriers and then transplanted into the dorsal side of nude mice.

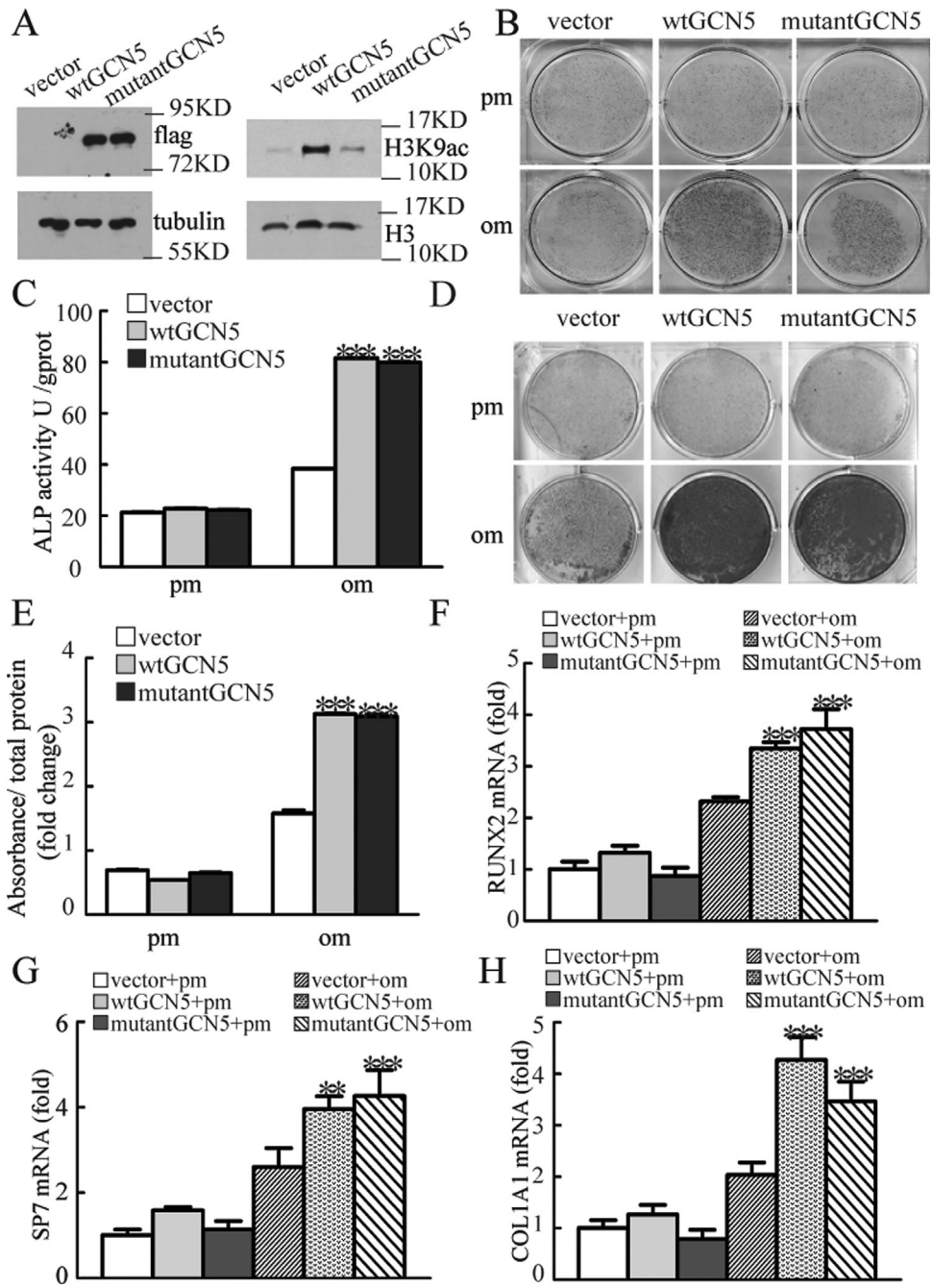

Fig. 2. Acetylase activity of GCN5 is dispensable for the regulation of osteogenic differentiation. (*A*) Rescue of WT or mutant GCN5 cell line was validated by Western blot. (*B*, *C*) Overexpression of GCN5 increased ALP activity in MSCs. Control, WT, or mutant GCN5 rescue cells were treated with proliferation or osteogenic media for 7 days for ALP staining (*B*), and cellular extracts were prepared to quantify ALP activity (*C*). (*D*, *E*) Overexpression of GCN5 promoted mineralization in MSCs. Cells with WT or mutant GCN5 overexpression were treated with proliferation or osteogenic media for 14 days, and then calcium deposition was observed using Alizarin Red S staining (*D*) and quantified (*E*). Overexpression of GCN5 promoted expression of *RUNX2* (*F*), *SP7* (*G*), and *COL1A1* (*H*) in MSCs as determined by RT-qPCR. All data are shown as the mean ± SD, $n = 3$. $^{**}p < 0.01$, $^{***}p < 0.001$. pm = proliferation media; om = osteogenic media.

After 6 weeks, transplants were harvested and prepared for histological analysis. H&E and Masson's trichrome staining showed that GCN5 knockdown cells formed less bone tissues than control cells and GCN5/p65 knockdown cells. Quantitative measurements demonstrated that the area of bone formation of the GCN5 knockdown group was significantly decreased ($p < 0.05$) compared with the control group and GCN5/p65 knockdown group (Fig. 4*E*, Supplemental Fig. 4C). As a whole, these results indicated the novel role of GCN5 in bone formation in a NF-κB–dependent manner.

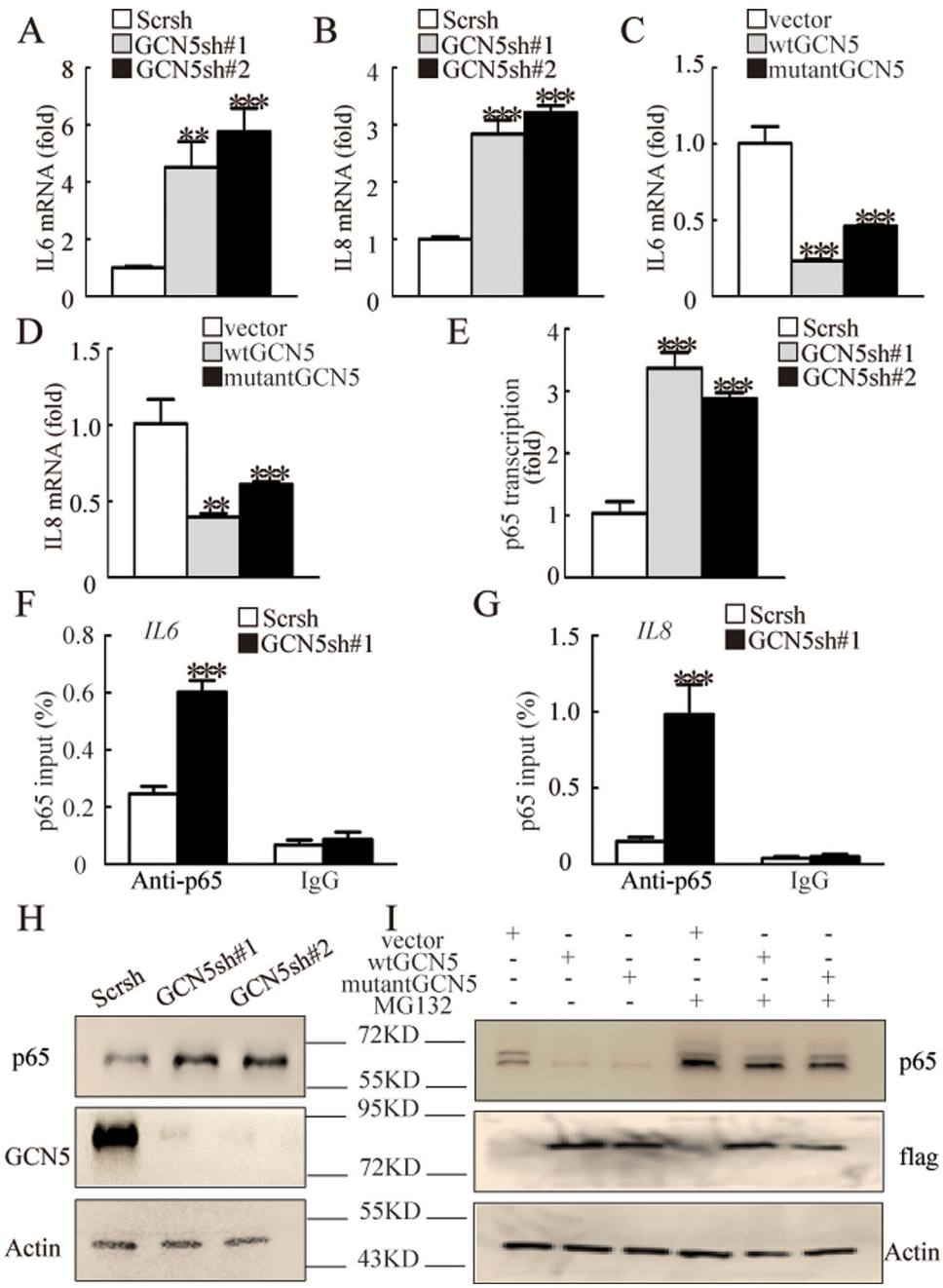

Fig. 3. GCN5 suppresses the NF-κB signaling pathway. (*A*, *B*) Knockdown of GCN5 increased *IL6* and *IL8* expression in MSCs as determined by RT-qPCR. (*C*, *D*) Both WT and mutant GCN5 inhibited *IL6* and *IL8* expression in MSCs as determined by RT-qPCR. (*E*) Knockdown of GCN5 promoted NF-κB transcription in MSCs as determined by luciferase reporter assay. (*F*, *G*) Occupancy of p65 on *IL6* and *IL8* gene promoters was analyzed by ChIP assay. (*H*) GCN5 deficiency was associated with enhanced p65 expression. Nuclear cell lysates of GCN5 knockdown cells were subjected to immunoblotting with anti-p65 antibody. (*I*) Whole-cell extracts were analyzed by immunoblotting after transfection with an empty plasmid or a plasmid expressing WT or mutant GCN5, in the presence or absence of MG132 (2 μM, for 12 hours). All data are shown as the mean ± SD, $n = 3$. $^{***}p < 0.001$. Scrsh = control cells; GCN5sh = GCN5 knockdown cells.

Decreased GCN5 in osteoporotic bone marrow

Based on our above experiments, we considered the possibility that GCN5 may be abnormally expressed in bone sections of osteoporotic mice. Therefore, we established the OVXed mouse model to test this hypothesis. μCT and H&E staining showed that the trabecular bone was significantly reduced in OVXed mice as compared with sham mice (Fig. 5*A–C*; Supplemental Fig. 5A, B). Next, histological and immunofluorescence analyses of femur sections from OVXed and sham mice were performed to detect GCN5 levels, and those of OVXed mice showed reduced GCN5 staining (Fig. 5*D*, *E*). Aged mice are also useful mouse models of osteoporosis. As shown in Fig. 5*F* and Supplemental Fig. 5C–F,

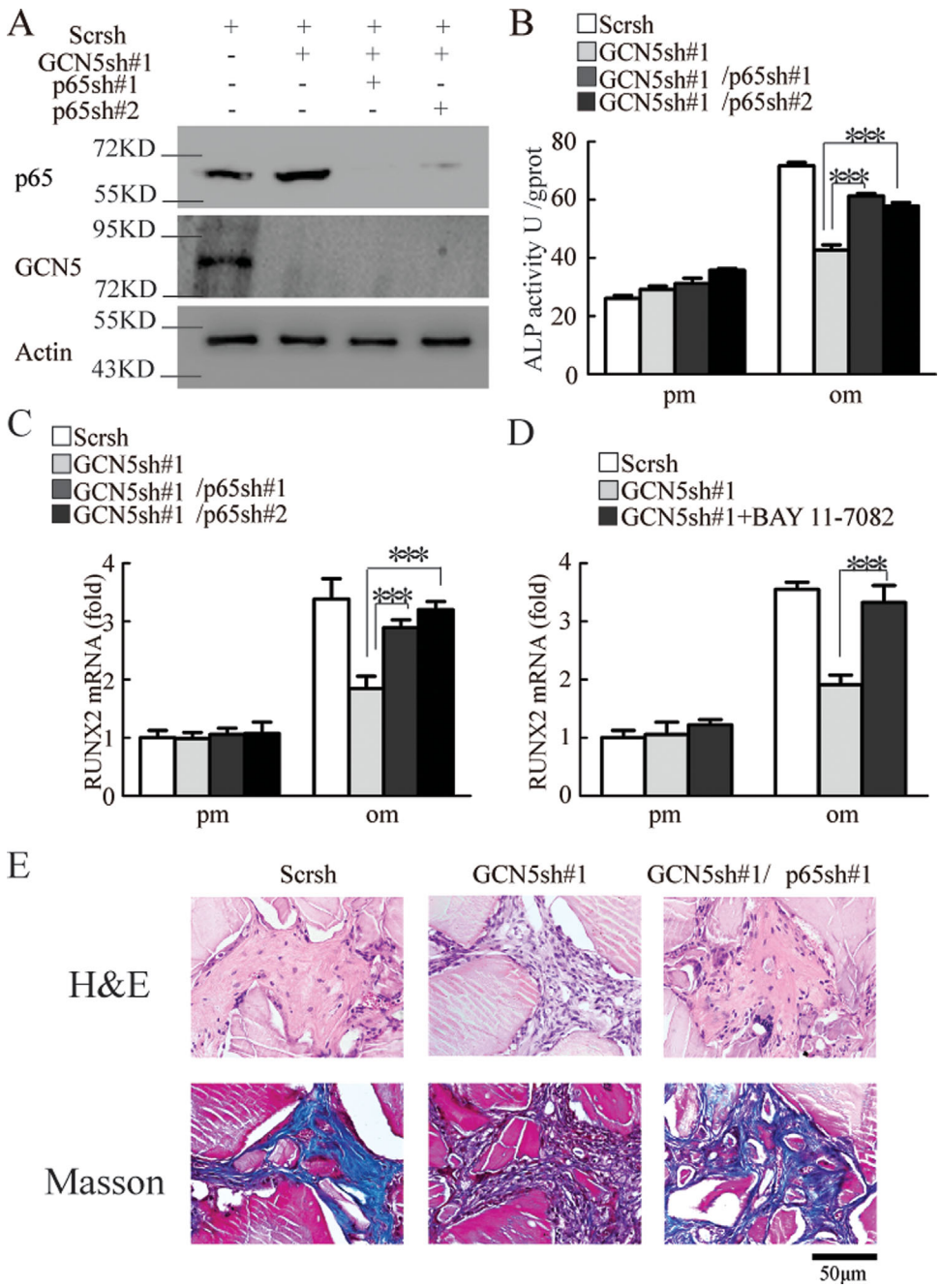

Fig. 4. GCN5 regulates osteogenic differentiation in a NF-κB–dependent manner. (*A*) Double knockdown of GCN5 and p65 was validated by Western blot. (*B*) ALP activity in control, GCN5 knockdown, and GCN5/p65 knockdown groups. (*C*) *RUNX2* expression in control, GCN5 knockdown, and GCN5/p65 knockdown groups was determined by RT-qPCR. (*D*) *RUNX2* expression in control, GCN5 knockdown, and GCN5 knockdown + BAY 11-7082 groups was determined by RT-qPCR. (*E*) H&E and Masson's trichrome staining of histological sections from implanted MSC-scaffold hybrids. Scale bar = 50 mm. All data are shown as the mean ± SD, $n = 3$. $^{***}p < 0.001$. pm = proliferation media; om = osteogenic media. Scrsh = control cells; GCN5sh = GCN5 knockdown cells; p65sh = p65 knockdown cells.

the trabecular bone morphometry showed significant bone loss in 16-month-old mice. To further confirm that GCN5 is associated with MSC fate commitments, we examined its status in bone sections of aged mice. Compared with younger 2-month-old mice, immunohistochemistry and confocal microscopy of femur sections in 16-month-old mice showed decreased GCN5 staining (Fig. 5*G*, *H*). Moreover, we observed increased p65 expression of femur sections in 16-month-old mice compared with younger 2-month-old mice (Supplemental Fig. 5G, H). Similarly, compared with sham mice, OVXed mice also showed increased p65 staining (Supplemental Fig. 6A, B). We also stained for actin in both

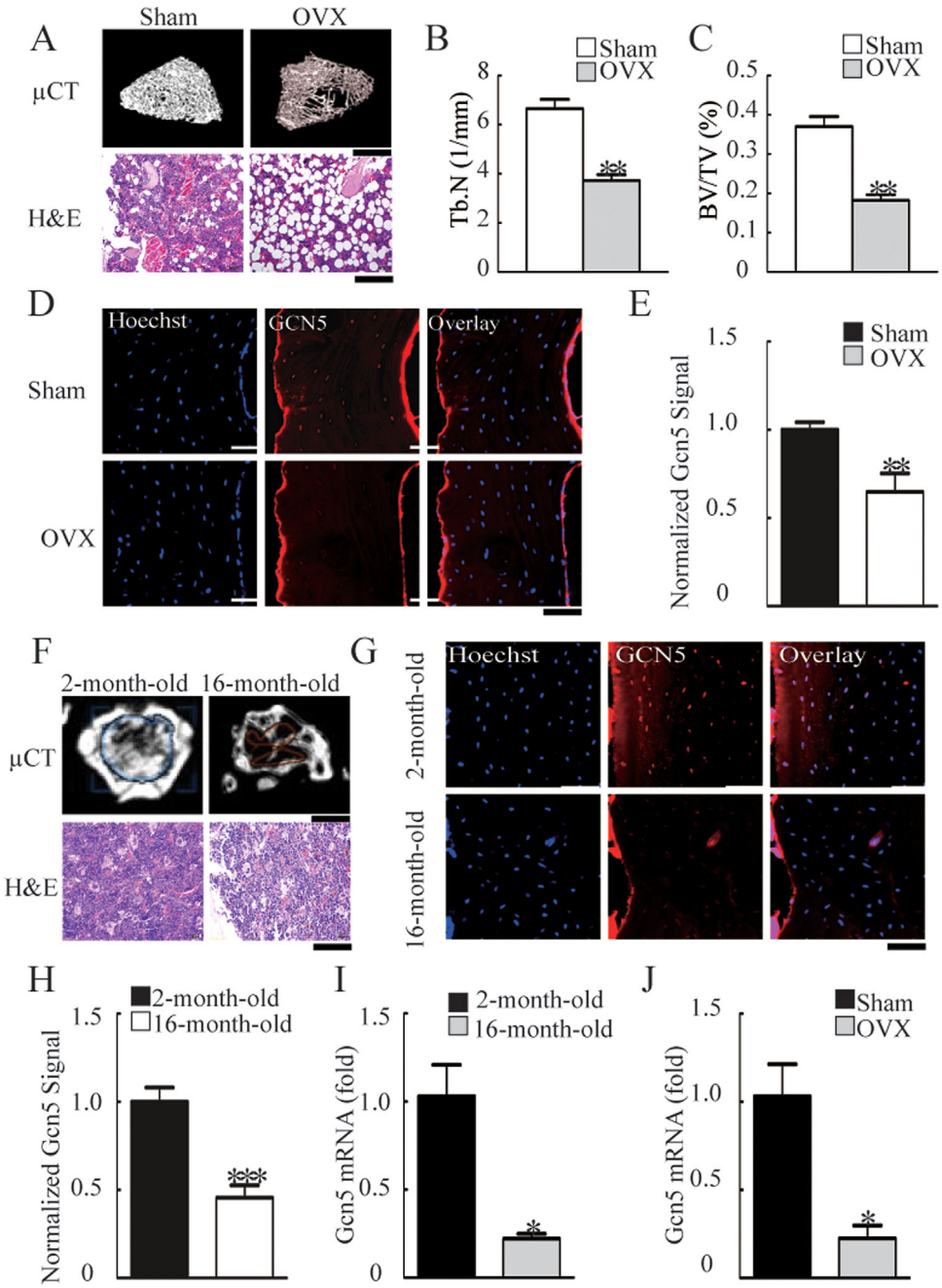

Fig. 5. Decreased GCN5 expression in osteoporotic bone marrow. Sixty mice were separated into four groups, with 15 mice per group (sham mice, OVXed mice, 2-month-old mice, and 16-month-old mice). (*A*) Representative μCT image and H&E staining of bone loss in OVXed mice. Scale bars for μCT and H&E represent 1 mm and 50 μm, respectively. (*B*) Trabecular number was reduced in OVXed mice. (*C*) Bone volume was reduced in OVXed mice. (*D*) Histology and immunofluorescence analyses of bone sections from OVXed mice showed decreased GCN5 expression compared with sham mice. Scale bar = 50 μm. (*E*) Quantification of normalized GCN5 signals in *D*. (*F*) Representative μCT image and H&E staining of bone loss in 16-month-old mice. Scale bars for μCT and H&E represent 1 mm and 20 μm, respectively. (*G*) Histology and immunofluorescence analyses of bone sections from 16-month-old mice showed decreased GCN5 expression compared with 2-month-old mice. Scale bar = 50 μm. (*H*) Quantification of normalized GCN5 signals in *G*. (*I*) Expression of *Gcn5* was reduced in MSCs from aged mice. (*J*) Expression of *Gcn5* was reduced in MSCs from OVXed mice compared with sham mice. All data are shown as the mean ± SD, $n = 3$. $^{**}p < 0.01$, $^{***}p < 0.001$.

sham and OVXed bone sections, and no difference was detected (Supplemental Fig. 6C). Moreover, no fluorescence was detected when the primary antibody was omitted as shown in Supplemental Fig. 6D.

Furthermore, we isolated MSCs from both 2-month-old and 16-month-old mice. Recently, mouse MSCs were found to express nestin, which could be utilized to directly detect MSCs in mouse bone marrow.[46] Many of the primary MSCs were

nestin-positive cells as observed by immunofluorescence staining (Supplemental Fig. 6E), and RT-qPCR revealed that the expression of *Gcn5* was decreased in MSCs from 16-month-old mice compared with those from 2-month-old mice (Fig. 5*I*). Compared with sham mice, MSCs from OVXed mice also displayed significantly reduced *Gcn5* expression (Fig. 5*J*). By contrast, expression of p65 target genes *Il6* and *Il8* increased in aged mice, whereas the *Icam1* expression displayed no significant change (Supplemental Fig. 6F–H).

Discussion

Our study demonstrated that GCN5 played an important role in osteogenic commitment of MSCs, revealing a previously uncharacterized function of the HAT GCN5. Interestingly, we observed cross-talk between GCN5 and NF-κB through investigation of the molecular mechanism. GCN5 was found to inhibit NF-κB signaling in MSCs, and most importantly, the HAT activity of GCN5 was determined to be not required for this process. In addition, experiments in OVXed and aged mouse models indicated that the metabolic bone disease osteoporosis was associated with abnormal expression of GCN5.

Upon differentiation of stem cells, relative levels of epigenetic markers change to reflect the activation and repression, guiding development toward one specific cell lineage. Histone acetylation has long been associated with transcriptionally active chromatin and histone deposition during DNA replication,[47,48] and it has been reported to be involved in osteogenesis recently. High levels of acetylated H3 and H4 histones during the proliferative period of osteoblast differentiation were observed in the promoter and coding region of the osteocalcin gene.[49] Moreover, downregulation of histone deacetylase could promote osteoblast differentiation.[50] However, the relationship between one specific HAT and the osteogenic commitment of MSCs has not been completely understood. In order to investigate the potential role of the HAT GCN5, we established GCN5 stable knockdown cells and detected that GCN5 deficiency impaired the osteogenic differentiation capability of MSCs (Fig. 1*A–I*, Supplemental Fig. 1B–G). However, contrary to our prediction, the GCN5 catalytically inactive acetyltransferase mutant was able to facilitate osteogenesis as well as WT GCN5 (Fig. 2). Previous genetic evidence indicated that GCN5 has HAT-independent functions. Deletion of GCN5 was shown to lead to embryonic death soon after gastrulation, whereas loss of GCN5 HAT activity caused neural tube closure defects.[51] A recent report also showed that GCN5/PCAF could repress IFN-β production and innate antiviral immunity in a HAT-independent and nontranscriptional manner.[52] As discussed above, a property of GCN5 was uncovered, which is separable from its known HAT activity in the current study.

In order to understand the molecular mechanism by which GCN5 promotes osteogenic differentiation of MSCs, we uncovered an unexpected crosstalk between GCN5 and NF-κB signaling in MSCs. GCN5-deficient cells demonstrated increased expression of NF-κB targeted genes (Fig. 3*A*, *B*; Supplemental Fig. 3A, B). This transcriptional inhibition was further confirmed by luciferase reporter and ChIP assays (Fig. 3*E–G*, Supplemental Fig. 3E). Consistent with our observations, another group reported the inhibition of NF-κB–mediated transcription by GCN5 in 293 and U2OS cells.[53] They indicated that GCN5 interacts with RelA and promotes its ubiquitination, and most importantly, GCN5-promoted RelA ubiquitination is separable from its known HAT activity or the function of its Bromo domain. Here, for the first time, we clarified that the suppression of NF-κB signaling by GCN5 occurred in a HAT activity–independent manner during osteogenic differentiation of MSCs (Fig. 3*C*, *D*; Supplemental Fig. 3C, D). Growing evidence suggests that NF-κB inhibits osteogenic differentiation of MSCs and bone formation in vivo. In the current study, both knockdown of p65 and treatment with the NF-κB inhibitor BAY 11-7082 were able to reverse the impaired osteogenic differentiation in GCN5 knockdown cells. Furthermore, bone formation experiments solidified our observations in vivo. Bio-Oss Collagen (Geistlich Pharma North America Inc., Princeton, NJ, USA) transplantation was used to identify the role of GCN5 and NF-κB in the nude mouse xenograft model. The collagen facilitates handling of the graft particles and acts to hold the Bio-Oss Collagen at the desired place. It acts as a framework onto which bone-forming cells and blood vessels can travel for formation of new bone.[54] Taking advantage of this system, we substantiated the function of GCN5 and NF-κB in vivo using H&E and Masson's trichrome staining.

Osteoporosis is one of the most common bone metabolic diseases that is associated with a shift in MSC lineage commitment. To examine the function of GCN5 in osteogenic differentiation of MSCs, we detected the expression of GCN5 in osteoporotic mice. Histological and immunofluorescence analyses of bone tissue sections revealed a significantly decreased GCN5 level in OVXed mice or aged mice (Fig. 5*D*, *G*). Combined with the in vitro data, the in vivo study suggests that decreased GCN5 contributes to the development of osteoporosis by influencing determination of MSC fate choices in the bone marrow.

Based on the present findings, we propose a novel role of GCN5 in the osteogenic commitment and development of osteoporosis. This novel function of GCN5 may provide valuable knowledge of the regulation of osteogenic differentiation of MSCs and benefit development of cell-based therapies for a diverse range of bone metabolic diseases.

Disclosures

All authors state that they have no conflicts of interest.

Acknowledgments

This study was supported by grants from the National Natural Science Foundation of China (No. 81570953, No. 81500822), the Program for New Century Excellent Talents in University from Ministry of Education (NCET-11-0026), the PKU School of Stomatology for Talented Young Investigators (PKUSS20140109), and the Construction Program for National Key Clinical Specialty from National Health and Family Planning Commission of China (2011).

Authors' roles: PZ: conception and design, collection and/or assembly of data, data analyses and interpretation, and manuscript writing; YL: collection and/or assembly of data and data analyses and interpretation; CJ: collection and/or assembly of data; MZ: collection and/or assembly of data; FT: financial support, provision of study material; YZ: conception and design, financial support, manuscript writing, and final approval of manuscript.

References

1. Prockop DJ. Marrow stromal cells as stem cells for nonhematopoietic tissues. Science. 1997;276(5309):71–4.
2. Chan CK, Seo EY, Chen JY, et al. Identification and specification of the mouse skeletal stem cell. Cell. 2015;160(1–2):285–98.
3. Worthley DL, Churchill M, Compton JT, et al. Gremlin 1 identifies a skeletal stem cell with bone, cartilage, and reticular stromal potential. Cell. 2015;160(1–2):269–84.
4. Horwitz EM, Gordon PL, Koo WK, et al. Isolated allogeneic bone marrow-derived mesenchymal cells engraft and stimulate growth in children with osteogenesis imperfecta: Implications for cell therapy of bone. Proc Natl Acad Sci U S A. 2002;99(13):8932–7.
5. Komori T, Yagi H, Nomura S, et al. Targeted disruption of Cbfa1 results in a complete lack of bone formation owing to maturational arrest of osteoblasts. Cell. 1997;89(5):755–64.
6. Mundlos S, Otto F, Mundlos C, et al. Mutations involving the transcription factor CBFA1 cause cleidocranial dysplasia. Cell. 1997;89(5):773–9.
7. Nakashima K, Zhou X, Kunkel G, et al. The novel zinc finger-containing transcription factor osterix is required for osteoblast differentiation and bone formation. Cell. 2002;108(1):17–29.
8. Zhou X, Zhang Z, Feng JQ, et al. Multiple functions of Osterix are required for bone growth and homeostasis in postnatal mice. Proc Natl Acad Sci U S A. 2010;107(29):12919–24.
9. Tontonoz P, Hu E, Graves RA, Budavari AI, Spiegelman BM. mPPAR gamma 2: tissue-specific regulator of an adipocyte enhancer. Genes Dev. 1994;8(10):1224–34.
10. Rosen ED, Sarraf P, Troy AE, et al. PPAR gamma is required for the differentiation of adipose tissue in vivo and in vitro. Mol Cell. 1999;4(4):611–7.
11. Wozney JM, Rosen V, Celeste AJ, et al. Novel regulators of bone formation: molecular clones and activities. Science. 1988;242(4885):1528–34.
12. Montero A, Okada Y, Tomita M, et al. Disruption of the fibroblast growth factor-2 gene results in decreased bone mass and bone formation. J Clin Invest. 2000;105(8):1085–93.
13. Tu X, Joeng KS, Nakayama KI, et al. Noncanonical Wnt signaling through G protein-linked PKCdelta activation promotes bone formation. Dev Cell. 2007;12(1):113–27.
14. Fuentealba LC, Eivers E, Ikeda A, et al. Integrating patterning signals: Wnt/GSK3 regulates the duration of the BMP/Smad1 signal. Cell. 2007;131(5):980–93.
15. Ambrosetti D, Holmes G, Mansukhani A, Basilico C. Fibroblast growth factor signaling uses multiple mechanisms to inhibit Wnt-induced transcription in osteoblasts. Mol Cell Biol. 2008;28(15):4759–71.
16. Mak KK, Bi Y, Wan C, et al. Hedgehog signaling in mature osteoblasts regulates bone formation and resorption by controlling PTHrP and RANKL expression. Dev Cell. 2008;14(5):674–88.
17. Ramasamy SK, Kusumbe AP, Wang L, Adams RH. Endothelial Notch activity promotes angiogenesis and osteogenesis in bone. Nature. 2014;507(7492):376–80.
18. Zhang H, Hilton MJ, Anolik JH, et al. NOTCH inhibits osteoblast formation in inflammatory arthritis via noncanonical NF-kappaB. J Clin Invest. 2014;124(7):3200–14.
19. Lawrence T, Bebien M, Liu GY, Nizet V, Karin M. IKKalpha limits macrophage NF-kappaB activation and contributes to the resolution of inflammation. Nature. 2005;434(7037):1138–43.
20. Rius J, Guma M, Schachtrup C, et al. NF-kappaB links innate immunity to the hypoxic response through transcriptional regulation of HIF-1alpha. Nature. 2008;453(7196):807–11.
21. Novack DV. Role of NF-kappaB in the skeleton. Cell Res. 2011;21(1):169–82.
22. Chang J, Wang Z, Tang E, et al. Inhibition of osteoblastic bone formation by nuclear factor-kappaB. Nat Med. 2009;15(6):682–9.
23. Chen Q, Liu K, Robinson AR, et al. DNA damage drives accelerated bone aging via an NF-kappaB-dependent mechanism. J Bone Miner Res. 2013;28(5):1214–28.
24. Chang J, Liu F, Lee M, et al. NF-kappaB inhibits osteogenic differentiation of mesenchymal stem cells by promoting beta-catenin degradation. Proc Natl Acad Sci U S A. 2013;110(23):9469–74.
25. Jimi E, Aoki K, Saito H, et al. Selective inhibition of NF-kappa B blocks osteoclastogenesis and prevents inflammatory bone destruction in vivo. Nat Med. 2004;10(6):617–24.
26. Vaira S, Alhawagri M, Anwisye I, Kitaura H, Faccio R, Novack DV. RelA/p65 promotes osteoclast differentiation by blocking a RANKL-induced apoptotic JNK pathway in mice. J Clin Invest. 2008;118(6):2088–97.
27. Brownell JE, Zhou J, Ranalli T, et al. Tetrahymena histone acetyltransferase A: a homolog to yeast Gcn5p linking histone acetylation to gene activation. Cell. 1996;84(6):843–51.
28. Imoberdorf RM, Topalidou I, Strubin M. A role for gcn5-mediated global histone acetylation in transcriptional regulation. Mol Cell Biol. 2006;26(5):1610–6.
29. Kim JH, Saraf A, Florens L, Washburn M, Workman JL. Gcn5 regulates the dissociation of SWI/SNF from chromatin by acetylation of Swi2/Snf2. Genes Dev. 2010;24(24):2766–71.
30. Kuo MH, Zhou J, Jambeck P, Churchill ME, Allis CD. Histone acetyltransferase activity of yeast Gcn5p is required for the activation of target genes in vivo. Genes Dev. 1998;12(5):627–39.
31. Govind CK, Zhang F, Qiu H, Hofmeyer K, Hinnebusch AG. Gcn5 promotes acetylation, eviction, and methylation of nucleosomes in transcribed coding regions. Mol Cell. 2007;25(1):31–42.
32. Howe L, Auston D, Grant P, et al. Histone H3 specific acetyltransferases are essential for cell cycle progression. Genes Dev. 2001;15(23):3144–54.
33. Wittschieben BO, Fellows J, Du W, Stillman DJ, Svejstrup JQ. Overlapping roles for the histone acetyltransferase activities of SAGA and elongator in vivo. EMBO J. 2000;19(12):3060–8.
34. Lin W, Zhang Z, Chen CH, Behringer RR, Dent SY. Proper Gcn5 histone acetyltransferase expression is required for normal anteroposterior patterning of the mouse skeleton. Dev Growth Differ. 2008;50(5):321–30.
35. Kahata K, Hayashi M, Asaka M, et al. Regulation of transforming growth factor-beta and bone morphogenetic protein signalling by transcriptional coactivator GCN5. Genes Cells. 2004;9(2):143–51.
36. Zhang P, Tu B, Wang H, et al. Tumor suppressor p53 cooperates with SIRT6 to regulate gluconeogenesis by promoting FoxO1 nuclear exclusion. Proc Natl Acad Sci USA. 2014;111(29):10684–9.
37. Ge W, Shi L, Zhou Y, et al. Inhibition of osteogenic differentiation of human adipose-derived stromal cells by retinoblastoma binding protein 2 repression of RUNX2-activated transcription. Stem Cells. 2011;29(7):1112–25.
38. Liu Y, Zhao Y, Zhang X, et al. Flow cytometric cell sorting and in vitro pre-osteoinduction are not requirements for in vivo bone formation by human adipose-derived stromal cells. PLoS One. 2013;8(2):e56002.
39. Ducy P, Desbois C, Boyce B, et al. Increased bone formation in osteocalcin-deficient mice. Nature. 1996;382(6590):448–52.
40. Weiss A, Arbell I, Steinhagen-Thiessen E, Silbermann M. Structural changes in aging bone: osteopenia in the proximal femurs of female mice. Bone. 1991;12(3):165–72.
41. Bouxsein ML, Boyd SK, Christiansen BA, Guldberg RE, Jepsen KJ, Muller R. Guidelines for assessment of bone microstructure in rodents using micro-computed tomography. J Bone Miner Res. 2010;25(7):1468–86.
42. Kennedy J, Baris C, Hoyland JA, Selby PL, Freemont AJ, Braidman IP. Immunofluorescent localization of estrogen receptor-alpha in growth plates of rabbits, but not in rats, at sexual maturity. Bone. 1999;24(1):9–16.
43. Lerin C, Rodgers JT, Kalume DE, Kim SH, Pandey A, Puigserver P. GCN5 acetyltransferase complex controls glucose metabolism through transcriptional repression of PGC-1alpha. Cell Metab. 2006;3(6):429–38.
44. Chen LF, Greene WC. Shaping the nuclear action of NF-kappaB. Nat Rev Mol Cell Biol. 2004;5(5):392–401.

45. Yeung F, Hoberg JE, Ramsey CS, et al. Modulation of NF-kappaB-dependent transcription and cell survival by the SIRT1 deacetylase. EMBO J. 2004;23(12):2369–80.
46. Mendez-Ferrer S, Michurina TV, Ferraro F, et al. Mesenchymal and haematopoietic stem cells form a unique bone marrow niche. Nature. 2010;466(7308):829–34.
47. Allfrey VG, Faulkner R, Mirsky AE. Acetylation and methylation of histones and their possible role in the regulation of RNA synthesis. Proc Natl Acad Sci U S A. 1964;51:786–94.
48. Allis CD, Chicoine LG, Richman R, Schulman IG. Deposition-related histone acetylation in micronuclei of conjugating Tetrahymena. Proc Natl Acad Sci U S A. 1985;82(23):8048–52.
49. Shen J, Hovhannisyan H, Lian JB, et al. Transcriptional induction of the osteocalcin gene during osteoblast differentiation involves acetylation of histones h3 and h4. Mol Endocrinol. 2003;17(4):743–56.
50. Lee HW, Suh JH, Kim AY, Lee YS, Park SY, Kim JB. Histone deacetylase 1-mediated histone modification regulates osteoblast differentiation. Mol Endocrinol. 2006;20(10):2432–43.
51. Bu P, Evrard YA, Lozano G, Dent SY. Loss of Gcn5 acetyltransferase activity leads to neural tube closure defects and exencephaly in mouse embryos. Mol Cell Biol. 2007;27(9):3405–16.
52. Jin Q, Zhuang L, Lai B, et al. Gcn5 and PCAF negatively regulate interferon-beta production through HAT-independent inhibition of T BK1. EMBO Rep. 2014;15(11):1192–201.
53. Mao X, Gluck N, Li D, et al. GCN5 is a required cofactor for a ubiquitin ligase that targets NF-kappaB/RelA. Genes Dev. 2009;23(7):849–61.
54. Wong RW, Rabie AB. Effect of bio-oss collagen and collagen matrix on bone formation. Open Biomed Eng J. 2010;4:71–6.